JACS
JOURNAL OF THE AMERICAN CHEMICAL SOCIETY
Article
pubs.acs.org/JACS

Bambusuril as a One-Electron Donor for Photoinduced Electron Transfer to Methyl Viologen in Mixed Crystals

Tomas Fiala,[†,‡,∥] Lucie Ludvíková,[†,‡,∥] Dominik Heger,[†,‡] Jan Švec,[†] Tomáš Slanina,[†,‡] L'ubica Vetráková,[†,‡] Michal Babiak,[†,§] Marek Nečas,[†] Petr Kulhánek,*[,‡,§] Petr Klán,*[,†,‡] and Vladimir Sindelar*[,†,‡]

[†]Department of Chemistry, Faculty of Science, Masaryk University, Kamenice 5, 625 00 Brno, Czech Republic
[‡]RECETOX, Faculty of Science, Masaryk University, Kamenice 5, 625 00 Brno, Czech Republic
[§]CEITEC - Central European Institute of Technology and National Centre for Biomolecular Research, Masaryk University, Kamenice 5, 625 00 Brno, Czech Republic

Supporting Information

ABSTRACT: Methyl viologen hexafluorophosphate ($MV^{2+}\cdot 2PF_6^-$) and dodecamethylbambus[6]uril (BU6) form crystals in which the layers of viologen dications alternate with those of a 1:2 supramolecular complex of BU6 and PF_6^-. This arrangement allows for a one-electron reduction of MV^{2+} ions upon UV irradiation to form $MV^{+\bullet}$ radical cations within the crystal structure with half-lives of several hours in air. The mechanism of this photoinduced electron transfer in the solid state and the origin of the long-lived charge-separated state were studied by steady-state and transient spectroscopies, cyclic voltammetry, and electron paramagnetic resonance spectroscopy. Our experiments are supported by quantum-chemical calculations showing that BU6 acts as a reductant. In addition, analogous photochemical behavior is also demonstrated on other MV^{2+}/BU6 crystals containing either BF_4^- or Br^- counterions.

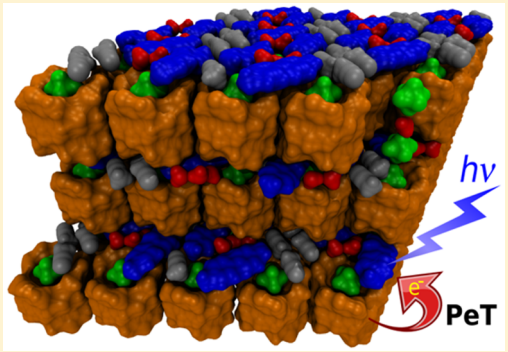

INTRODUCTION

Photoinduced electron transfer (PeT) processes have been intensively studied for their importance in many fields, such as the development of solar cells and light-emitting diodes.[1−5] The key reaction intermediate in such applications is a long-lived photoinduced charge-separated state of a radical pair. Methyl viologen (MV^{2+}) and other dialkylbipyridinium derivatives are a well-known class of organic dications that can be stepwise reduced to give the corresponding radical cations or neutral forms.[6−9] Such a reduction can be accomplished thermally or photochemically and is reversible. The rate of thermal reverse electron transfer is usually very high, which precludes the use of these systems for solar energy conversion. However, it has been shown that stabilization of viologen radical cations can be achieved by their incorporation to solid matrices, such as zeolites,[10,11] polymers,[12,13] Langmuir−Blodgett monolayers,[14] crystal frameworks,[15−18] and hybrid structures.[19−21]

Bambusurils are a family of macrocyclic compounds whose first derivatives were reported by some of us in 2010.[22] These macrocycles were recognized as anion receptors, showing a high affinity and selectivity toward various anions in both organic solvents and aqueous media.[23−27] For these properties, bambusurils have been used in conjunction with NMR spectroscopy and mass spectrometry to analyze multicomponent anion mixtures.[25,28] Interestingly, these macrocycles can not only bind spherical anions such as halides but also engulf weakly coordinating anions such as BF_4^- and PF_6^-. We recently demonstrated that dodecamethylbambus[6]uril (BU6) (Figure 1a) crystallizes in the presence of tetrabutylammonium (TBA) halide salts to form crystals in which the layers of BU6−halide complexes are separated from those of TBA cations.[27]

Here we report that substitution of TBA halide salt with methyl viologen hexafluorophosphate ($MV^{2+}\cdot 2PF_6^-$) results in a photoactive crystalline material in which the organic macrocycle, BU6, acts as an electron donor in photoreduction of MV^{2+}. A combined experimental−computational study was carried out to explain this phenomenon.

RESULTS AND DISCUSSION

Crystal Structure Analyses. Light-yellow crystals were obtained upon slow crystallization of a solution of BU6 and excess $MV^{2+}\cdot 2PF_6^-$ in a water/acetonitrile (1:1) mixture. X-ray crystallography revealed that the crystals contain a supramolecular complex of BU6, MV^{2+}, and PF_6^- (**BU6**/**MV^{2+}**/**PF_6^-**; Figure 1a−c). Two PF_6^- anions occupy each of the two entrances of the BU6 cavity. The fluorine atom F′ (Figure 1b) of each of the opposing PF_6^- ions is nested deep into the BU6 cavity and interacts with the H−C^2 and H−C^6 methine

Received: August 17, 2016
Published: February 13, 2017

DOI: 10.1021/jacs.6b08589
J. Am. Chem. Soc. 2017, 139, 2597−2603

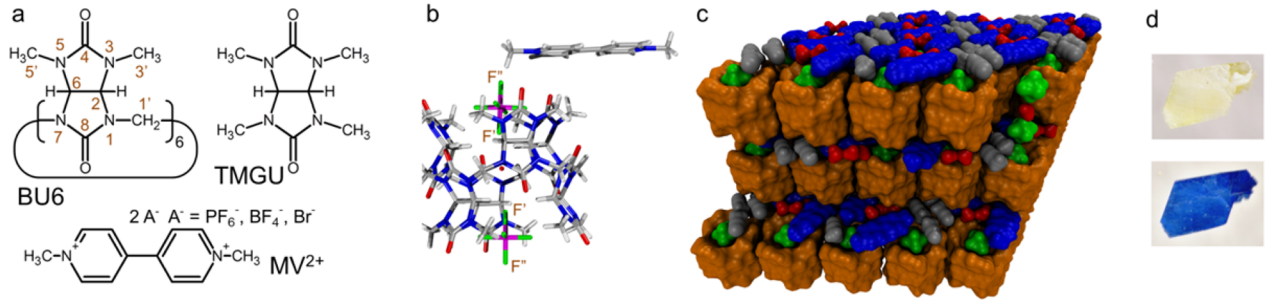

Figure 1. (a) Compounds used in this study. (b) Part of the X-ray structure of **BU6/MV^{2+}/PF$_6^-$** crystal. (c) Packing of the crystal structure of **BU6/MV^{2+}/PF$_6^-$** crystal (BU6, orange; MV^{2+}, blue; PF$_6^-$, green; acetonitrile, gray; water, red). (d) Photographs showing **BU6/MV^{2+}/PF$_6^-$** crystals before (top) and after (bottom) UV irradiation.

hydrogen atoms of the macrocycle, forming weak C−H···F hydrogen bonds, the shortest H···F distance being 2.57 Å.

The complex is further stabilized by one water molecule, which is situated in the cavity center between two PF$_6^-$ anions. A similar stabilization of anions inside the BU6 cavity has been reported before.[24,29] In this paper, an arrangement formed by BU6, two PF$_6^-$ anions, and one water molecule between the anions is denoted as the BC^{2-} complex. In the crystal, the BC^{2-} complexes form layers in which neighboring BU6 macrocycles interact by weak N^1−CH···O=C^8 and N^3−CH···O=C^4 hydrogen bonds, with the shortest H···O distance being 2.69 Å. Moreover, the layers are further stabilized by the dipole−dipole interactions of the C^8=O carbonyl groups that are in the anti orientation at the interface of two adjacent macrocycles.

The layers containing the BC^{2-} complexes alternate with the layers formed by the MV^{2+} ions and acetonitrile and water molecules. Thus, two types of layers exist within the crystal structure: one bearing a positive charge and the other one a negative charge (Figure 1c). A similar charge separation in adjacent layers within the crystal has previously been described for complexes between BU6 and halide anions in the form of tetrabutylammonium salts.[30] The MV^{2+} molecules are positioned in close proximity to BU6. At least one oxygen atom in both BU6 portals reaches one of the aromatic rings of MV^{2+} with an average C···O distance of approximately 3 Å. The thicknesses of the cationic and anionic layers defined by planes passing through the centers of fluorine atoms F″ (Figure 1b) placed outside the macrocycles are 2.98 and 11.35 Å, respectively.

Altogether, the unit cell of triclinic shape contains three MV^{2+} ions, three BC^{2-} complexes, and four acetonitrile and six water molecules (a total of 591 atoms). All of the molecules within the unit cell are very well packed without any voids that would allow for diffusion of oxygen or other gases into the crystal.

In addition, we decided to study mixed crystals based on BU6 and MV^{2+} containing different counterions, such as BF$_4^-$ and Br$^-$. Thus, analogous **BU6/MV^{2+}/BF$_4^-$** and **BU6/MV^{2+}/Br$^-$** crystals were prepared. X-ray diffractometry revealed several differences among the three types of prepared crystals (Figures 1, S1 and S2). Unlike the PF$_6^-$ ions, BF$_4^-$ and Br$^-$ are centered inside the BU6 macrocycles and form inclusion complexes with 1:1 stoichiometry. In the **BU6/MV^{2+}/BF$_4^-$** crystals, the complex adopts a layered structure similar to that of **BU6/MV^{2+}/PF$_6^-$**. The thicknesses of the anionic and cationic layers defined by planes passing through the centers of the oxygen atoms at the BU6 portals are 9.57 and 4.85 Å, respectively; the analogous distances in **BU6/MV^{2+}/PF$_6^-$** are 9.59 and 4.76 Å. The layers are parallel to the crystallographic *ac* plane; along the *a* direction, the MV^{2+} cations are arranged in distinct channels that are separated by parallel channels of a solvent (methanol).

BU6/MV^{2+}/Br$^-$ crystals do not have a layered structure. Instead, the main structural unit is composed of two axially aligned BU6·Br$^-$ complexes sharing a MV^{2+} ion between them; the cation axis is parallel to those of the anions, and several weak interactions, including C$_{sp^3}$−H···O interactions, stabilize a face-centered orientation of the MV^{2+} plane with respect to the BU6 external side walls. Such structural units in the crystal are connected through numerous interactions between the carbonyl oxygens and CH$_3$/CH$_2$ hydrogen atoms of neighboring BU6 macrocycles.

Photochemical Properties of Mixed Crystals. Irradiation of the three mixed crystals **BU6/MV^{2+}/PF$_6^-$**, **BU6/MV^{2+}/BF$_4^-$**, and **BU6/MV^{2+}/Br$^-$** with UV light (using a continuous laser with λ = 375 nm) resulted in an immediate color change from light yellow to blue (Figure 1d; the same color change occurs upon irradiation at 266 nm). The blue color of all three forms of intact crystals persisted over at least 5 h before it reverted back to the light-yellow color in both the air and nitrogen atmosphere. To study the nature of this blue color, the crystals were crushed to obtain homogeneous powder for diffuse reflectance (DR) studies. DR spectra for all three mixed crystals exhibited two new bands with maxima at 398 and 607 nm (Figures 2a and S3).

This color change was studied as the remission function ($f(R)$) difference on crushed **BU6/MV^{2+}/PF$_6^-$** crystals, initially irradiated at 375 nm for 1 h in the air atmosphere (Figure S4a) and subsequently left in the dark (Figure S4b). The same DR spectral change (light-yellow crystals ⇄ blue crystals) was observed for seven repetitions, and we concluded that the process is fully reversible (Figure 3).

In the next step, the kinetics of the measured remission function change in the crushed **BU6/MV^{2+}/PF$_6^-$** crystals was investigated at 298 K. The DR spectra of the irradiated sample at 375 nm in the air atmosphere were recorded every 5 min for 6 h after the light source was turned off. The observed $f(R)$ decay was best fitted by the kinetic model A → D, B → D, and C → D with three first-order rate constants of (1.78 ± 0.05) × 10^{-3}, (4.66 ± 0.30) × 10^{-4}, and (8.56 ± 0.81) × 10^{-5} s^{-1} (Figure S5a). After the decay was complete, the same sample was kept under the flow of nitrogen to avoid air oxygen and irradiated at 375 nm for 1 h. The spectra were recorded every 30 min for 24 h. The observed decay was best fitted by the kinetic model A → C and B → C with two first-order rate

DOI: 10.1021/jacs.6b08589
J. Am. Chem. Soc. 2017, 139, 2597−2603

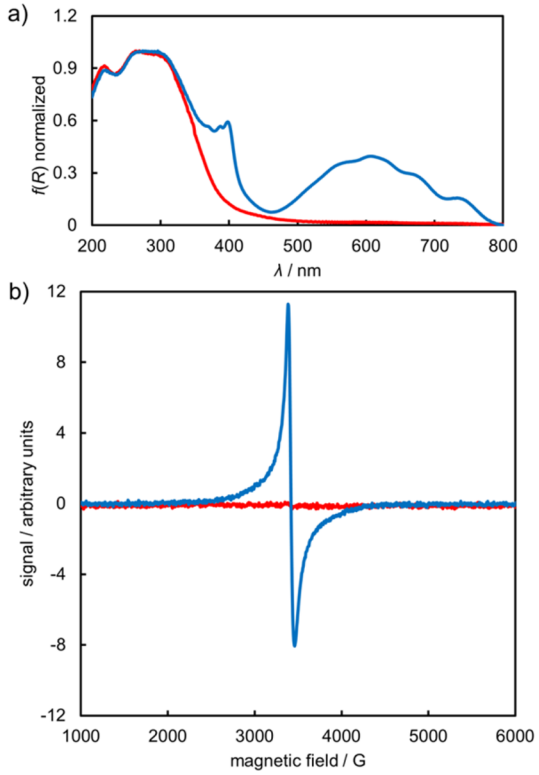

Figure 2. (a) UV–vis diffuse reflectance spectra and (b) EPR spectra of **BU6/MV^{2+}/PF$_6^-$** before (red) and after (blue) UV irradiation.

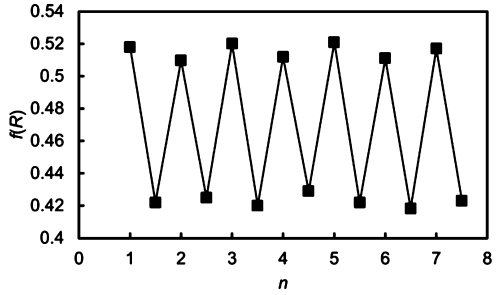

Figure 3. Reversible changes in the remission function monitored at 398 nm upon a periodic 1 h irradiation of crushed **BU6/MV^{2+}/PF$_6^-$** crystals followed by keeping the sample in the dark for 1 h (n is the number of repetitions). The solid line is a guide for the eyes.

constants of $(1.63 \pm 0.32) \times 10^{-3}$ and $(4.89 \pm 0.27) \times 10^{-5}$ s^{-1} (Figure S5b).

Decay rate constants of the same magnitude were observed for **BU6/MV^{2+}/BF$_4^-$** crystals: $(6.07 \pm 0.78) \times 10^{-3}$, $(9.93 \pm 0.55) \times 10^{-4}$, and $(1.82 \pm 0.04) \times 10^{-4}$ s^{-1} in the case of the aerated sample and $(3.10 \pm 0.02) \times 10^{-4}$ and $(2.93 \pm 0.19) \times 10^{-5}$ s^{-1} in the case of the sample kept under nitrogen.

The normalized kinetic traces observed at 610 nm for **BU6/MV^{2+}/PF$_6^-$** and **BU6/MV^{2+}/BF$_4^-$** irradiated at 375 nm under different conditions are shown in Figure 4. These results clearly demonstrate that the observed decay is strongly influenced by the presence of oxygen but not by the anion type or a different crystal packing. In general, the observed half-life of the colored state of the crushed crystals in the absence of oxygen was ca. 2 h, which is shorter but still on the same order of magnitude as that of intact crystals. However, the half-life of crushed crystals in the presence of oxygen was only ca. 10 min.

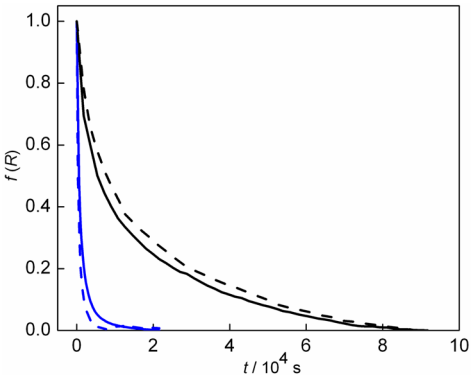

Figure 4. Normalized kinetic traces of $f(R)$ for crushed crystals of **BU6/MV^{2+}/PF$_6^-$** (solid lines) and **BU6/MV^{2+}/BF$_4^-$** (dashed lines) crystals observed in air (blue) and nitrogen (black) atmosphere.

Long lifetimes of metastable transient species photogenerated in the crystalline state via electron transfer have been observed when a back electron transfer process is restricted.[16,31,32] We hypothesized that the color change observed in this work is connected with a photoinduced reduction of MV^{2+} to give the viologen radical cation (MV$^{+\bullet}$) and that the long-lived radical ion pair (RIP) thereby formed can be of triplet multiplicity or, simply, there is no reasonable mechanism available for oxidation of MV$^{+\bullet}$ to MV^{2+}. Indeed, the two bands of the remission function, λ_{max} = 398 and 607 nm, in the diffuse reflectance spectrum (Figure 2a) match those of the absorption and diffuse reflectance spectra already reported for MV$^{+\bullet}$ in both solution and the solid state.[6−9]

Oxidation of MV$^{+\bullet}$ to MV^{2+} by atmospheric oxygen is known to be fast and efficient in solution.[33,34] This process should be restricted in intact crystals, as the majority of the viologen molecules are incorporated inside the crystal with tight crystal packing, preventing diffusion of oxygen molecules toward the reactive radical ion intermediates (see above). However, crushing the material probably caused disruption of the crystal structure and allowed for the observation of a substantial quenching effect of the colored state by oxygen, suggesting that oxidation of MV$^{+\bullet}$ occurs. Inhomogeneous destruction of the crystals is also probably responsible for the observation of multiple quenching rate constants, which can be interpreted by the presence of more or less disrupted crystalline entities in the sample. Nevertheless, the decrease in the observed half-life is clearly related to the presence of oxygen. The fact that the process was fully reversible and no chemical changes in the studied system upon repeated photolysis were observed suggests that quenching of a triplet state is involved.

Additional evidence for the presence of long-lived MV$^{+\bullet}$ was obtained from steady-state EPR experiments in the solid state. While the crystals before irradiation were EPR-silent, the EPR spectrum of the blue crystals exhibited a strong single resonance at g = 2.0047 (Figure 2b).

Nature of the Electron Donor. The main question that remained at this point was the mechanism of MV$^{+\bullet}$ formation. MV^{2+}, as the key chromophore in the crystal, absorbs a photon to form an excited singlet state, which acts as a strong oxidizing agent.[35] It has already been demonstrated that in acetonitrile, excited MV^{2+} oxidizes molecules that possess gas-phase ionization potentials (IPs) lower than 10.3 eV.[35] Because acetonitrile, water, and PF$_6^-$ possess IPs higher than this threshold (>12.2 eV), they should not play any role in the

DOI: 10.1021/jacs.6b08589
J. Am. Chem. Soc. 2017, 139, 2597−2603

observed PeT process.[35] Thus, the reducing agent that could donate an electron to form $MV^{+\bullet}$ can only be BU6.

In order to confirm that the excited singlet MV^{2+} could be reduced by BU6 in a mixed crystal, we studied this reaction spectroscopically in an acetonitrile solution. Because the lifetime of the excited singlet state of MV^{2+} in the solution is very short,[36] picosecond transient absorption spectroscopy was used. In addition, a structurally related 2,4,6,8-tetramethylglycoluril (TMGU) (Figure 1a) possessing a comparable oxidation potential and good acetonitrile solubility was used instead of the poorly soluble BU6. Deactivation pathways of the excited singlet state of MV^{2+} in both the absence and the presence of TMGU were investigated. In the absence of TMGU, the initial transient absorption spectrum, determined by the global analysis of the measured data, was assigned to the excited singlet state of MV^{2+} (Figure 5, blue line; two absorption maxima at 325 and 385 nm). The maximum at 385 nm corresponds to that previously reported by Kohler and coworkers,[35] whereas the signal at 325 nm was out of their study range. In agreement with their observation, we found no evidence of photoreduction of the MV^{2+} excited singlet state (i.e., formation of $MV^{+\bullet}$) by acetonitrile. A new species, assigned to $MV^{+\bullet}$ according to the literature,[6−9] was observed for samples of MV^{2+} (1 mM) in acetonitrile containing TMGU at different concentrations (c = 10, 30, 54, and 100 mM) after the laser pulse. The global analysis of the spectral data with a model of the single-exponential kinetic function gave observed rate constants for $MV^{+\bullet}$ formation in the range of $(1-5) \times 10^9$ s^{-1}. Because such an observed rate constant is higher than that typical for a diffusion-controlled process, we assumed that electron transfer occurs within a ground-state associate. Indeed, the association constant of methyl viologen and TMGU in acetonitrile determined by UV−vis spectroscopy (for details, see Figure S6) was found to be (348 ± 75) M^{-1}. This constant was then used to calculate analytical concentrations of the complex under the same experimental conditions as those used in the transient spectroscopy measurements (see the Supporting Information). The correlation between the complex concentrations and the spectral absorbance of $MV^{+\bullet}$ at 392 nm, obtained as a final spectrum from the global analysis of the measured data, is high (Figure S7). Thus, we conclude that reduction of the excited singlet state of MV^{2+}, involving electron transfer, occurs only within the complex of methyl viologen and TMGU and, subsequently, the two reactants form a radical ion pair.

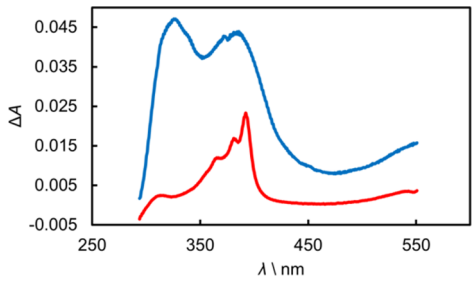

Figure 5. Transient absorption spectra of the excited singlet state of MV^{2+} (blue line) and $MV^{+\bullet}$ (red line) obtained by photolysis of an acetonitrile solution of MV^{2+} and TMGU. The spectra were determined by the global analysis of the measured data in 120 ps steps up to a 1.8 ns delay after the pump pulse.

In addition, the UV−vis absorption spectra of MV^{2+}/TMGU solutions were recorded before and after irradiation at 266 nm. An increase in the absorption intensity in the region of 300−400 nm is apparent in Figure S8 as an indication of the photoproduct(s) formation. We did not perform any detailed product analysis but assumed that the products are a dimer of $MV^{+\bullet}$ or doubly reduced MV^{2+}, which have been reported to be formed under similar conditions[35] and absorb in the same region as the photoproducts observed in our experiments.

Cyclic voltammetry of TMGU in an acetonitrile solution showed an irreversible oxidation peak with a half-wave potential of $E_{1/2}$ = +2.10 V vs SCE (using ferrocene as an internal standard).[36] This oxidation potential is comparable to that of unsubstituted urea (ca. +1.90 V vs SCE in water;[37] a typical voltammogram is shown in Figure S9). Although BU6 did not exhibit a distinct oxidation peak, presumably because of the presence of two similar types of nitrogen atoms in its structure, we were able to determine that its oxidation occurs at approximately +2.2 V vs SCE, which matches the oxidation potential of TMGU. We also calculated the driving force for the one-electron reduction potential of a methyl viologen/BU6 couple to support our experimental data. The excited-state reduction potential of methyl viologen is $E(MV^{2+}*/MV^{+\bullet})$ = +3.65 V vs SCE. This value was estimated from its ground-state potential, $E(MV^{2+}/MV^{+\bullet})$ = −0.45 V vs SCE[38] and the energy of the excited singlet state of MV^{2+}, E_S = 396 kJ mol^{-1} (ca. 4.104 eV).[35] As the oxidation potential of BU6 was determined to be −2.2 V vs SCE, the Gibbs energy of electron transfer between the excited singlet of MV^{2+} and BU6, ΔG_{eT}, equals ca. −1.45 eV (ca. −140 kJ mol^{-1}), and thus, the process is exergonic.

The results from our experiments provide sufficient evidence that the appearance of blue color in the crystals is a consequence of efficient one-electron transfer from BU6 to the excited singlet state of methyl viologen, probably followed by formation of a triplet radical ion pair. However, they do not provide a clear explanation why the resulting RIP is long-lived. Therefore, we decided to use quantum-chemical calculations to reveal the nature of the RIP and clarify the mechanism of its formation.

Quantum-Chemical Calculations. We employed theoretical modeling to determine whether the RIP can be formed in the triplet state, which would explain its long-lived nature, as the reverse electron transfer is an inefficient spin-forbidden process. We calculated energies of all possible singlet and triplet states that can be involved in the RIP formation (Figure S10; see the Supporting Information for details). We were especially focused on evaluating the intersystem crossing (ISC) efficiencies of all possible steps that can produce the triplet state by calculating the singlet−triplet (S−T) splitting and spin−orbit coupling (SOC).[39] In our calculations, we considered two key components of the **BU6/MV^{2+}/PF_6^-** mixed crystal, MV^{2+} and BC^{2-}, and several types of models, which are described in detail in the Supporting Information.

On the basis of our experimental findings, we suggested that the most probable mechanism consists of the following steps:

$$MV^{2+}{\cdot}BC^{2-} \xrightarrow{h\nu} {}^1LE(MV) \xrightarrow{eT} {}^1RIP \xrightarrow{ISC} {}^3RIP \xrightarrow{eT} MV^{2+}{\cdot}BC^{2-}$$

In the first step, the initial state ($MV^{2+}{\cdot}BC^{2-}$) is excited by light to the locally excited (LE) singlet state of methyl viologen ($^1LE(MV)$). This state has sufficient energy (4.19 eV) to initiate oxidation of BU6 to form the singlet state of the $MV^{+\bullet}$·

DOI: 10.1021/jacs.6b08589
J. Am. Chem. Soc. 2017, 139, 2597−2603

$BC^{-\bullet}$ radical ion pair (^{1}RIP). The calculated energy change for the ^{1}LE(MV) → ^{1}RIP step, ΔE_{eT} = −2.19 eV (−211.3 kJ mol^{-1}), is higher than the experimentally determined value of ΔG_{eT} (ca. −1.45 eV; see above) for a similar process in the solution. Such a difference could be attributed to thermal effects that are omitted in our calculations. A larger value can also indicate that the oxidized form of BU6 is stabilized more efficiently because of the presence of the PF_6^- anions in the BU6 cavity compared with the stabilization of TMGU in acetonitrile. This type of stabilization is also supported by the calculated difference in the electron density obtained upon BU6 oxidation (Figure S11), which shows that the positive charge in $BU6^{+\bullet}$ is localized on the top and bottom rims of the macrocycle in the very close vicinity of anions found in the supramolecular assembly of $BC^{-\bullet}$.

The singlet and triplet states of RIP (^{1}RIP and ^{3}RIP, 2.05 and 1.95 eV) are the lowest electronically excited states of the given multiplicity of the entire unit cell (initial state) of the mixed crystal. This confirms that once the RIP is formed, it can convert back to the initial state only by a single electron transfer process. The S−T splitting calculated for the RIP is very small (ca. 0.1 eV), indicating that ^{1}RIP can efficiently undergo ISC to give the long-lived triplet state ^{3}RIP. Moreover, the splittings of the $MV^{+\bullet}$ and $BC^{-\bullet}$ singly occupied molecular orbitals due to the SOC are 0.39 and 0.12 eV, respectively, showing a larger difference than that found for the MV^{2+}* state (see the Supporting Information). ^{3}RIP is then responsible for the blue coloration of the mixed crystal because it contains methyl viologen in the reduced form. Because ^{3}RIP ($MV^{+\bullet}$·$BC^{-\bullet}$) has to be EPR-active, we calculated isotropic values of the **g** tensors for the $MV^{+\bullet}$ and $BC^{-\bullet}$ moieties in vacuum, which are 2.0030 and 2.0062, respectively. The experimentally observed value of 2.0047 matches their average value (2.0046), suggesting that the long-lived ^{3}RIP is indeed detected during EPR measurements.

Finally, the experimentally observed long half-life of the formed ^{3}RIP is explained by an inefficient, spin-forbidden back electron transfer transition (^{3}RIP → MV^{2+}·BC^{2-}) whose probability is further reduced by a large energy separation of the triplet and singlet states (ca. 1.95 eV) and possibly by limited geometry relaxation of the RIP within the mixed crystal.

We also characterized pathways leading to ^{3}RIP by the electronic excitations of BU6 in the BC^{2-} supramolecular assembly. Our calculations indicate that although BC^{2-}* (Figure S10) exhibits efficient ISC and could induce electron transfer, the probability of this process is very low because the probability of BC^{2-} excitation is 1−2 orders of magnitude lower than that of methyl viologen. In addition, the impact of the type of anion on the stability of $BU6^{+\bullet}$ was studied in the series of (a) BC^{2-}, (b) a complex of BU6 and Br^-, and (c) BU6 (as a reference) in vacuum. Energies required to form $BU6^{+\bullet}$ are +266.7, +473.0, and +710.2 kJ mol^{-1}, respectively (see the Supporting Information for details). On the other hand, we found that the presence of anions in the BU6 cavity does not influence the S−T splitting in the locally excited state of BU6, which is very small (ca. 0.01 eV). These data indicate that anions might influence the stability of a RIP with respect to the initial state but do not influence the ISC efficiency, which is in accordance with our experimental findings.

CONCLUSION

We have demonstrated that MV^{2+} in the form of its PF_6^- salt and the neutral macrocyclic compound BU6 packed in mixed crystals can undergo photoinduced electron transfer. We have shown that BU6 acts as a source of electrons to reduce MV^{2+}* to the $MV^{+\bullet}$ radical. The radicals formed are stable inside intact crystals in air for several hours before the initial state is restored. The photoinduced electron transfer cycle can be repeated several times without significant loss of its efficiency. The same process was observed in two other types of crystals containing both MV^{2+} and BU6 but different types of anion and crystal packing.

The reversible formation of long-lived radicals via charge separation is appealing because of its relevance to energy-storage systems. This work shows that glycoluril-based macrocycles can be used as electron donors in a PeT process. To the best of our knowledge, no example of a glycoluril-based macrocycle enabling an electron-transfer reaction has been reported to date.

EXPERIMENTAL AND COMPUTATIONAL METHODS

Preparation and Characterization of the Mixed Crystals. All of the X-ray diffraction data were measured at 120 K on a Rigaku diffractometer (rotating anode, partial χ-axis goniometer, CCD detector) using Mo Kα radiation (λ = 0.71075 Å). CCDC 1413477, 1521355, and 1521356 contain the supplementary crystallographic data for this paper. These data can be obtained free of charge from The Cambridge Crystallographic Data Centre via www.ccdc.cam.ac.uk/data_request/cif.

BU6/MV^{2+}/PF$_6^-$ Crystals. Methyl viologen hexafluorophosphate (MV^{2+}·$2PF_6^-$) (135 mg, 284 mmol), dodecamethylbambus[6]uril (BU6) (103 mg, 94 mmol), water (7 mL), and acetonitrile (7 mL) were sonicated for 5 min. Undissolved solid was filtered off, and the resulting solution was left to stand in a dark place for 2 weeks at room temperature, during which time the solvents partially evaporated. The resulting mixture contained light-yellow crystals of the BU6−MV^{2+}·$2PF_6^-$ complex (76 mg) and colorless needles of pure MV^{2+}·$2PF_6^-$ (50 mg). The crystals were collected by filtration and separated manually.

Crystallographic data for BU6·(MV^{2+}·$2PF_6^-$)·$^4/_3CH_3CN$·$2H_2O$·H_2O ($C_{56.67}H_{84}F_{12}N_{27.33}O_{15}P_2$): M_r = 1678.11, crystal dimensions 0.21 mm × 0.16 mm × 0.16 mm, space group $P\bar{1}$, a = 17.8727(2) Å, b = 18.7412(2) Å, c = 19.8363(3) Å, α = 66.3210(10)°, β = 67.0100(10)°, γ = 69.4060(10)°, V = 5449.88 Å^3, Z = 3, ρ_{calcd} = 1.534 g cm^{-3}, μ = 0.174 mm^{-1}; 64 075 reflections collected, 20 454 unique reflections (R_{int} = 0.0128), data/restraints/parameters 20454/542/1742, final R indices ($I > 2\sigma(I)$) R_1 = 0.0617 and wR_2 = 0.1792, $\Delta\rho_{max}/\Delta\rho_{min}$ = 1.24/−0.77 e Å^{-3}.

BU6/MV^{2+}/Br$^-$ Crystals. Methyl viologen chloride (MV^{2+}·$2Cl^-$·xH_2O) (18 mg, 70 μmol based on the dry form), BU6·HCl complex (20 mg, 18 μmol), 46% aqueous HBr solution (4.2 μL, 36 μmol of HBr), MeOH (4 mL), and CH_2Cl_2 (4 mL) were sonicated for 10 min. Undissolved solid was filtered off, and the resulting solution was left to stand in a dark place for 1 month at room temperature, during which time the solvents partially evaporated, yielding light-yellow crystals of the BU6−($^1/_2MV^{2+}$·Br^-) complex.

Crystallographic data for BU6·($^1/_2MV^{2+}$·Br^-) ($C_{48}H_{67}BrN_{25}O_{12}$): M_r = 1266.17, space group $P2_1/c$, a = 19.3696(2) Å, b = 15.39990(10) Å, c = 24.2089(2) Å, β = 94.0220(10)°, V = 7203.49(11) Å^3, Z = 4, ρ_{calcd} = 1.168 g cm^{-3}, μ = 0.637 mm^{-1}; 109 866 reflections collected, 13 494 unique reflections (R_{int} = 0.0423), data/restraints/parameters 13494/45/788, final R indices ($I > 2\sigma(I)$) R_1 = 0.0548 and wR_2 = 0.1574, $\Delta\rho_{max}/\Delta\rho_{min}$ = 1.47/−0.82 e Å^{-3}.

BU6/MV^{2+}/BF$_4^-$ Crystals. Methyl viologen tetrafluoroborate (MV^{2+}·$2BF_4^-$) (64 mg, 180 μmol), BU6·HCl complex (40 mg, 36 μmol), MeOH (4 mL), and CH_2Cl_2 (4 mL) were sonicated for 10 min. Undissolved solid was filtered off, and the resulting solution was left to stand in a dark place for 1 month at room temperature, during

DOI: 10.1021/jacs.6b08589
J. Am. Chem. Soc. 2017, 139, 2597−2603

which time the solvents partially evaporated, yielding light-yellow crystals of the BU6–($^{1}/_{2}MV^{2+}\cdot BF_4^-$) complex.

Crystallographic data for BU6·($^{1}/_{2}MV^{2+}\cdot BF_4^-$)·4$CH_3OH$ ($C_{52}H_{83}BF_4N_{25}O_{16}$): M_r = 1401.24, space group $P\bar{1}$, a = 11.9917(3) Å, b = 15.2680(5) Å, c = 21.2185(5) Å, α = 95.821(2)°, β = 91.000(2)°, γ = 107.853(3)°, V = 3673.90(18) Å^3, Z = 2, ρ_{calcd} = 1.267 g cm^{-3}, μ = 0.102 mm^{-1}; 47 137 reflections collected, 13 784 unique reflections (R_{int} = 0.0436), data/restraints/parameters 13784/78/950, final R indices ($I > 2\sigma(I)$) R_1 = 0.0623 and wR_2 = 0.1853, $\Delta\rho_{max}/\Delta\rho_{min}$ = 0.40/−0.29 e Å^{-3}.

Diffuse Reflectance Spectra. UV–vis diffuse reflectance spectra were measured in the reaction chamber of a Harrick Praying Mantis Diffuse Reflection Accessory coupled with an Agilent Cary 5000 spectrophotometer. The reaction chamber allowed measurements under various atmospheres by purging gas through the chamber. The crystals were crushed in a mortar with a pestle, placed into the chamber, and irradiated with a 375 nm laser. After irradiation, diffuse reflectance spectra were measured at different times. A white standard (packed $BaSO_4$) was used as a reference. The measured reflectance spectra were converted to the remission function $f(R) = (1 - R)^2/2R$, where R is the reflectance of the sample. The rate constants were determined by global analysis using a Levenberg–Marquardt algorithm. A larger error margin in the constants obtained for samples kept under nitrogen occurred because the observed decay was not complete.

Picosecond Transient Spectroscopy. Picosecond transient absorption was measured using the pump–supercontinuum probe technique. The system was equipped with a Ti:sapphire laser system (775 nm, pulse energy 1.0 mJ, full width at half-maximum <150 fs, operating frequency 425.6 Hz). Part of the beam was fed into a noncollinear optical parametric amplifier. The output at 532 nm was compressed to <50 fs pulses, and its frequency was doubled by a β-barium borate (BBO) crystal to 266 nm with pulse energy of 1.6 μJ. The probe beam was generated by focusing the 775 nm beam into a CaF_2 plate with a 4 mm path length, which produced a supercontinuum spanning a wavelength range of 270–620 nm. The pump and probe beams were focused to a 0.2 mm spot on the sample that circulated in an optical cell with a thickness of <1 mm. The probe beam and a reference signal obtained by passing the solution next to the pump beam were spectrally dispersed and registered with two NMOS sensors (512 pixels). The pump–probe cross-correlation was <100 fs over the entire spectrum. To improve the signal-to-noise ratio, the data were averaged over multiple pump–probe scans (three to six scans with 400 shots per temporal point). All of the transient absorption spectra were measured on a 1 mM solution of MV^{2+} in acetonitrile in 15 ps steps up to a delay of 1.8 ns. Data were analyzed by global analysis of the time-resolved transient absorption spectra to obtain species spectra and the first-order rate constants.

Electrochemistry. The cyclic voltammetry measurements were performed in acetonitrile (TMGU or BU6, c = 1 mM) containing 0.1 M tetra-*n*-butylammonium hexafluorophosphate as a conducting salt using ferrocene/ferrocenium (Fc/Fc^+, 1 mM) as an internal standard under an argon atmosphere. A glassy carbon working electrode, a platinum wire counter electrode, and an Ag wire quasi-reference electrode were employed. The measurements were carried out at a scan rate of 50 mV s^{-1}.

Computational Methods. Details of the calculations are provided in the Supporting Information. The atom positions and unit cell dimensions were taken from the structure determined by X-ray crystallography. The initial model was refined employing molecular modeling, and its geometry was further optimized using the CPMD package[40] at the PBE/70Ry level of theory[41] with a correction for dispersion interactions according to Grimme.[42] The optimization was done at constant volume, employing periodic boundary conditions at the Γ point of the Brillouin zone. The energy and electronic properties of the R, ^{1}RIP, and ^{3}RIP states were calculated at PBE/100Ry level of theory by employing the restricted open-shell Kohn–Sham theory[43] to describe the ^{1}RIP and ^{3}RIP states.

The properties of MV^{2+}, BC^{2-}, $MV^{+\bullet}$, $BC^{-\bullet}$, BU6, and BU6·Br^- were determined in vacuum on optimized geometries or on specified geometries at the PBE/TZ2P[44] level of theory in the ADF package.[45] The initial geometries were taken from the optimized model of the crystal structure. The electronic transitions obtained by the TD-DFT approach[46,47] and EPR properties[48,49] were calculated with inclusion of relativistic effects by the scalar zero-order regular approximation (ZORA). The strength of spin–orbit coupling was determined from the full and scalar ZORA calculations.[50]

The properties of the neutral and oxidized forms of BU6 were calculated on the geometry-optimized structure in the Gaussian 09 package[51] at the PBE/6-31G* level of theory.[52,53] The difference in the electron densities of the oxidized and neutral forms and the spin density in the oxidized form were visualized using VMD.[54]

■ ASSOCIATED CONTENT

Supporting Information

The Supporting Information is available free of charge on the ACS Publications website at DOI: 10.1021/jacs.6b08589.

Additional results and computational details (PDF)
Crystallographic data for **BU6/MV^{2+}/PF$_6^-$** (CIF)
Crystallographic data for **BU6/MV^{2+}/BF$_4^-$** (CIF)
Crystallographic data for **BU6/MV^{2+}/Br$^-$** (CIF)
Optimized geometries (ZIP)

■ AUTHOR INFORMATION

Corresponding Authors

*kulhanek@chemi.muni.cz
*klan@chemi.muni.cz
*sindelar@chemi.muni.cz

ORCID

Petr Klán: 0000-0001-6287-2742
Vladimir Sindelar: 0000-0003-0090-5961

Author Contributions

‖T.F. and L.L. contributed equally.

Notes

The authors declare no competing financial interest.

■ ACKNOWLEDGMENTS

This work was supported by the Czech Science Foundation (13-15576S) and the Ministry of Education, Youth and Sports of the Czech Republic (LQ1601, LO1214, and LM2015051). We acknowledge the CF X-ray diffraction and Bio-SAXS supported by the CIISB research infrastructure (LM2015043 funded by MEYS CR). Computational resources were provided by the CESNET (LM2015042) and the CERIT Scientific Cloud (LM2015085) under the program "Projects of Large Research, Development, and Innovations Infrastructures". We thank Dr. Lorant Szatmary for measuring EPR spectra and Dr. Karel Kubíček and Dr. Dušan Hemzal for discussions in the early stage of this project.

■ REFERENCES

(1) Tvrdy, K.; Frantsuzov, P. A.; Kamat, P. V. *Proc. Natl. Acad. Sci. U. S. A.* **2011**, *108*, 29–34.
(2) Szendrei, K.; Cordella, F.; Kovalenko, M. V.; Böberl, M.; Hesser, G.; Yarema, M.; Jarzab, D.; Mikhnenko, O. V.; Gocalinska, A.; Saba, M.; Quochi, F.; Mura, A.; Bongiovanni, G.; Blom, P. W. M.; Heiss, W.; Loi, M. A. *Adv. Mater.* **2009**, *21*, 683–687.
(3) Zhou, Y.; Eck, M.; Krüger, M. *Energy Environ. Sci.* **2010**, *3*, 1851–1864.
(4) Lazorski, M. S.; Gest, R. H.; Elliott, C. M. *J. Am. Chem. Soc.* **2012**, *134*, 17466–17469.

DOI: 10.1021/jacs.6b08589
J. Am. Chem. Soc. 2017, 139, 2597–2603

(5) Yui, T.; Kobayashi, Y.; Yamada, Y.; Yano, K.; Fukushima, Y.; Torimoto, T.; Takagi, K. *ACS Appl. Mater. Interfaces* **2011**, *3*, 931−935.
(6) Kosower, E. M.; Cotter, J. L. *J. Am. Chem. Soc.* **1964**, *86*, 5524−5527.
(7) Yoon, K. B.; Kochi, J. K. *J. Am. Chem. Soc.* **1988**, *110*, 6586−6588.
(8) Bockman, T.; Kochi, J. *J. Org. Chem.* **1990**, *55*, 4127−4135.
(9) Alvaro, M.; Garcia, H.; Garcia, S.; Marquez, F.; Scaiano, J. C. *J. Phys. Chem. B* **1997**, *101*, 3043−3051.
(10) Álvaro, M.; Ferrer, B.; García, H.; Hashimoto, S.; Hiratsuka, M.; Asahi, T.; Masuhara, H. *ChemPhysChem* **2004**, *5*, 1058−1062.
(11) Álvaro, M.; Bizzoca, G.; Ferrer, B.; García, H.; de Miguel, M.; Teruel, L. *ChemPhysChem* **2010**, *11*, 3456−3464.
(12) Nakashima, K.; Miyamoto, T.; Hashimoto, S. *Chem. Commun.* **1999**, 213−214.
(13) Suzuki, M.; Kimura, M.; Shirai, H. *Chem. Commun.* **1997**, 2061−2062.
(14) Li, J.-Y.; Peng, M.-L.; Zhang, L.-P.; Wu, L.-Z.; Wang, B.-J.; Tung, C.-H. *J. Photochem. Photobiol., A* **2002**, *150*, 101−108.
(15) Zhang, Q.; Wu, T.; Bu, X.; Tran, T.; Feng, P. *Chem. Mater.* **2008**, *20*, 4170−4172.
(16) Yoshikawa, H.; Nishikiori, S.; Watanabe, T.; Ishida, T.; Watanabe, G.; Murakami, M.; Suwinska, K.; Luboradzki, R.; Lipkowski, J. *J. Chem. Soc., Dalton Trans.* **2002**, 1907−1917.
(17) Abouelwafa, A. S.; Mereacre, V.; Balaban, T. S.; Anson, C. E.; Powell, A. K. *CrystEngComm* **2010**, *12*, 94−99.
(18) Yao, Q.-X.; Ju, Z.-F.; Jin, X.-H.; Zhang, J. *Inorg. Chem.* **2009**, *48*, 1266−1268.
(19) Yui, T.; Kobayashi, Y.; Yamada, Y.; Yano, K.; Fukushima, Y.; Torimoto, T.; Takagi, K. *ACS Appl. Mater. Interfaces* **2011**, *3*, 931−935.
(20) Tagliazucchi, M.; Tice, D. B.; Sweeney, C. M.; Morris-Cohen, A. J.; Weiss, E. A. *ACS Nano* **2011**, *5*, 9907−9917.
(21) Wu, K.; Li, Q.; Jia, Y.; McBride, J. R.; Xie, Z.; Lian, T. *ACS Nano* **2015**, *9*, 961−968.
(22) Svec, J.; Necas, M.; Sindelar, V. *Angew. Chem., Int. Ed.* **2010**, *49*, 2378−2381.
(23) Havel, V.; Svec, J.; Wimmerova, M.; Dusek, M.; Pojarova, M.; Sindelar, V. *Org. Lett.* **2011**, *13*, 4000−4003.
(24) Havel, V.; Sindelar, V.; Necas, M.; Kaifer, A. E. *Chem. Commun.* **2014**, *50*, 1372−1374.
(25) Yawer, M. A.; Havel, V.; Sindelar, V. *Angew. Chem., Int. Ed.* **2015**, *54*, 276−279.
(26) Révész, Á.; Schröder, D.; Svec, J.; Wimmerová, M.; Sindelar, V. *J. Phys. Chem. A* **2011**, *115*, 11378−11386.
(27) Svec, J.; Dusek, M.; Fejfarova, K.; Stacko, P.; Klán, P.; Kaifer, A. E.; Li, W.; Hudeckova, E.; Sindelar, V. *Chem. - Eur. J.* **2011**, *17*, 5605−5612.
(28) Havel, V.; Yawer, M. A.; Sindelar, V. *Chem. Commun.* **2015**, *51*, 4666−4669.
(29) Fiala, T.; Sindelar, V. *Supramol. Chem.* **2016**, *28*, 810−816.
(30) Svec, J.; Dusek, M.; Fejfarova, K.; Stacko, P.; Klán, P.; Kaifer, A. E.; Li, W.; Hudeckova, E.; Sindelar, V. *Chem. - Eur. J.* **2011**, *17*, 5605−5612.
(31) Abouelwafa, A. S.; Mereacre, V.; Balaban, T. S.; Anson, C. E.; Powell, A. K. *CrystEngComm* **2010**, *12*, 94−99.
(32) Yao, Q.-X.; Ju, Z.-F.; Jin, X.-H.; Zhang, J. *Inorg. Chem.* **2009**, *48*, 1266−1268.
(33) Farrington, J. A.; Ebert, M.; Land, E. J. *J. Chem. Soc., Faraday Trans. 1* **1978**, *74*, 665.
(34) Stradowski, C. *J. Appl. Polym. Sci.* **1990**, *41*, 2511−2512.
(35) Peon, J.; Tan, X.; Hoerner, J. D.; Xia, C.; Luk, Y. F.; Kohler, B. *J. Phys. Chem. A* **2001**, *105*, 5768−5777.
(36) Pavlishchuk, V. V.; Addison, A. W. *Inorg. Chim. Acta* **2000**, *298*, 97−102.
(37) Cataldo Hernández, M.; Russo, N.; Panizza, M.; Spinelli, P.; Fino, D. *Diamond Relat. Mater.* **2014**, *44*, 109−116.
(38) Nolan, J. E.; Plambeck, J. A. *J. Electroanal. Chem. Interfacial Electrochem.* **1990**, *294*, 1−20.
(39) Marian, C. M. *Wiley Interdiscip. Rev. Comput. Mol. Sci.* **2012**, *2*, 187−203.
(40) *CPMD*, version 3.17.1; http://www.cpmd.org/; Copyright IBM Corp 1990−2008, Copyright MPI fur Festkoperforschung Stuttgart 1997−2001.
(41) Perdew, J. P.; Burke, K.; Ernzerhof, M. *Phys. Rev. Lett.* **1996**, *77*, 3865−3868.
(42) Grimme, S. *J. Comput. Chem.* **2006**, *27*, 1787−1799.
(43) Frank, I.; Hutter, J.; Marx, D.; Parrinello, M. *J. Chem. Phys.* **1998**, *108*, 4060−4069.
(44) Van Lenthe, E.; Baerends, E. J. *J. Comput. Chem.* **2003**, *24*, 1142−1156.
(45) *ADF 2014.10*; Scientific Computing & Modelling NV: Amsterdam, 2015; http://www.scm.com.
(46) van Gisbergen, S. J. A.; Snijders, J. G.; Baerends, E. J. *Comput. Phys. Commun.* **1999**, *118*, 119−138.
(47) Rosa, A.; Baerends, E. J.; van Gisbergen, S. J. A.; van Lenthe, E.; Groeneveld, J. A.; Snijders, J. G. *J. Am. Chem. Soc.* **1999**, *121*, 10356−10365.
(48) van Lenthe, E.; Wormer, P. E. S.; van der Avoird, A. *J. Chem. Phys.* **1997**, *107*, 2488.
(49) van Lenthe, E.; van der Avoird, A.; Wormer, P. E. S. *J. Chem. Phys.* **1998**, *108*, 4783.
(50) van Lenthe, E.; van Leeuwen, R.; Baerends, E. J.; Snijders, J. G. *Int. J. Quantum Chem.* **1996**, *57*, 281−293.
(51) Frisch, M. J.; Trucks, G. W.; Schlegel, H. B.; Scuseria, G. E.; Robb, M. A.; Cheeseman, J. R.; Scalmani, G.; Barone, V.; Mennucci, B.; Petersson, G. A.; Nakatsuji, H.; Caricato, M.; Li, X.; Hratchian, H. P.; Izmaylov, A. F.; Bloino, J.; Zheng, G.; Sonnenberg, J. L.; Hada, M.; Ehara, M.; Toyota, K.; Fukuda, R.; Hasegawa, J.; Ishida, M.; Nakajima, T.; Honda, Y.; Kitao, O.; Nakai, H.; Vreven, T.; Montgomery, J. A., Jr.; Peralta, J. E.; Ogliaro, F.; Bearpark, M.; Heyd, J. J.; Brothers, E.; Kudin, K. N.; Staroverov, V. N.; Kobayashi, R.; Normand, J.; Raghavachari, K.; Rendell, A.; Burant, J. C.; Iyengar, S. S.; Tomasi, J.; Cossi, M.; Rega, N.; Millam, J. M.; Klene, M.; Knox, J. E.; Cross, J. B.; Bakken, V.; Adamo, C.; Jaramillo, J.; Gomperts, R.; Stratmann, R. E.; Yazyev, O.; Austin, A. J.; Cammi, R.; Pomelli, C.; Ochterski, J. W.; Martin, R. L.; Morokuma, K.; Zakrzewski, V. G.; Voth, G. A.; Salvador, P.; Dannenberg, J. J.; Dapprich, S.; Daniels, A. D.; Farkas, Ö.; Foresman, J. B.; Ortiz, J. V.; Cioslowski, J.; Fox, D. J. *Gaussian 09*, revision D.01; Gaussian, Inc.: Wallingford, CT, 2009.
(52) Hehre, W. J.; Ditchfield, R.; Pople, J. A. *J. Chem. Phys.* **1972**, *56*, 2257.
(53) Hariharan, P. C.; Pople, J. A. *Theor. Chim. Acta* **1973**, *28*, 213−222.
(54) Humphrey, W.; Dalke, A.; Schulten, K. *J. Mol. Graphics* **1996**, *14*, 33−38.

DOI: 10.1021/jacs.6b08589
J. Am. Chem. Soc. 2017, 139, 2597−2603